Tuberculosis 118 (2019) 101854

Contents lists available at ScienceDirect

Tuberculosis

journal homepage: www.elsevier.com/locate/tube

Mechanisms of Pathogenesis

Effects of membrane lipid composition on *Mycobacterium tuberculosis* EsxA membrane insertion: A dual play of fluidity and charge

Supriyo Ray[a,**], Salvador Vazquez Reyes[b,c], Chuan Xiao[a,c], Jianjun Sun[b,c,*]

[a] Department of Chemistry, University of Texas at El Paso, 500 West University Avenue, El Paso, TX, 79968, USA
[b] Department of Biological Sciences, University of Texas at El Paso, 500 West University Avenue, TX, 79968, USA
[c] Border Biomedical Research Center at University of Texas at El Paso, 500 West University Avenue, TX, 79968, USA

ARTICLE INFO

Keywords:
Mycobacterium tuberculosis
ESAT-6
EsxA
Lipid composition
Membrane insertion

ABSTRACT

As a key virulence factor of *Mycobacterium tuberculosis*, EsxA or 6-kDa early secreted antigenic target (ESAT-6) has been implicated in phagosome rupture and mycobacterial translocation from the phagosome to the cytosol within macrophages. Our previous studies have shown that EsxA permeabilizes liposomal membrane at acidic pH and a membrane-permeabilization defective mutant Q5K attenuates mycobacterial cytosolic translocation and virulence in macrophages. To further probe the mechanism of EsxA membrane permeabilization, here we characterized the effects of various lipid compositions, including biologically relevant phagosome-mimicking lipids and lipid rafts, on the structural stability and membrane insertion of EsxA WT and Q5K. We have found a complex dual play of membrane fluidity and charge in regulating EsxA membrane insertion. Moreover, Q5K affects the membrane insertion through a structure- and lipid composition-independent mechanism. The results of this study provide a novel insights into the mechanism of EsxA membrane interaction.

1. Introduction

Mycobacterium tuberculosis (*Mtb*), the causative agent of tuberculosis (TB), accounts for more than one million death worldwide each year [1,2]. Upon inhalation into lungs, *Mtb* is recognized and internalized by alveolar macrophages through phagocytosis. Within the phagosomes, *Mtb* exhibits the ability of inhibiting phagosome-lysosome fusion, persisting and replicating within the phagosomes [3–7]. Recently, evidence has been found that upon phagosome-lysosome fusion, *Mtb* progressively translocates from the phago-lysosomes into the cytosol, a favorable place for *Mtb* to replicate and spread to new cells [4,8–13]. The ability of arresting phagosomal maturation and translocating to the cytosol has been attributed, at least in part, to the *esx-1* locus that encodes the bacterial Type VII secretion system [14]. Earlier comparative genomic studies discovered the Region of Difference 1 (RD1) that is present in *Mtb* but absent in the attenuated vaccine strain *Mycobacterium bovis* Bacille Calmette-Guérin (BCG) [15,16]. Deletion of RD1 from *Mtb* resulted in attenuation of virulence and retention of mycobacteria in the phagosome, while transfer of RD1 into BCG partially restored virulence [17–22]. The RD1 is located within the *esx-1* locus that encodes the ESX-1 secretion system and two secreted effector proteins: EsxA (formerly 6-kDa early-secreted antigenic target (ESAT-6) or Rv3875) and EsxB (formerly 10-kDa culture filtrate protein (CFP-10) or Rv3874) [23–26]. EsxA and EsxB form a heterodimer and are secreted out of *Mtb* in a co-dependent manner [27].

EsxA was first discovered in the short-term culture filtrate of *Mtb* as a potent T-cell antigen [23]. It has been intensively studied as a novel vaccine candidate against TB [28–30]. Recently, compelling evidence obtained by genetic approaches, such as knock out or knock in of EsxA gene, have shown that EsxA is an essential virulence factor for *Mtb* pathogenesis and particularly required for mycobacterial cytosolic translocation, intracellular replicating and cell-to-cell spreading [8–10,12]. Earlier biochemical studies have shown that EsxA has a membrane-lytic activity. In a planar lipid bilayer system, either EsxA alone or in combination with EsxB caused disruption of the artificial membranes [19]. EsxA, but not EsxB, exhibited strong association with the liposomes and lysed the liposomes at acidic pH [31].

In the past several years, we have been systematically investigating the mechanism of EsxA and EsxB membrane interaction. We have shown that upon acidification EsxA, but not EsxB, undergoes dramatic conformational change and disrupts liposomal membranes [32]. We have obtained the direct evidence that EsxA inserts into lipid membranes with its two α-helixes forming a membrane-spanning domain [33]. We have also found that the orthologous EsxA from non-

* Corresponding author. Department of Biological Sciences, University of Texas at El Paso, 500 500 West University Avenue, TX, 79968, USA.
** Corresponding author.
E-mail addresses: sray4@utep.edu (S. Ray), jsun@utep.edu (J. Sun).

https://doi.org/10.1016/j.tube.2019.07.005
Received 1 February 2019; Received in revised form 26 July 2019; Accepted 29 July 2019
Available online 30 July 2019
1472-9792/ © 2019 Elsevier Ltd. All rights reserved.

pathogenic *Mycobacterium smegmatis* (*Ms*), which shares over 76% homology with EsxA from *Mtb*, is inactive in membrane interaction [32,34]. All the findings suggest that the membrane-permeabilizing activity of EsxA is a major determinant for virulence phenotypes of mycobacterial species [34,35]. Most recently, we have presented evidence that a single-residue mutation Q5K of EsxA compromised the membrane-permeabilizing activity and attenuated mycobacterial virulence in macrophages and in zebra fish embryos through inhibiting mycobacterial cytosolic translocation [36].

While the role of EsxA in *Mtb* cytosolic translocation has been well established, the molecular mechanism of EsxA membrane insertion is little understood. It is not clear how the Q5K mutation causes defects in EsxA membrane insertion. An earlier study has shown that EsxA had a strong association with the liposomes containing dimyristoylphosphatidylcholine (DMPC) and cholesterol [31]. Moreover, it has been reported that *Mtb* utilized lipid raft aggregates for internalization into alveolar epithelial cells [37]. Thus, lipid composition appears to be an important factor influencing EsxA binding and/or inserting into the membrane.

In the present study, we characterize the effects of pH, temperature and lipid compositions on structural stability and membrane insertion of EsxA WT and Q5K mutant. The results have revealed a dual play of membrane fluidity and charge in regulation of EsxA membrane insertion.

2. Materials and methods

Lipids: 1-palmitoyl-2-oleoyl-*sn*-glycero-3- phosphocholine (POPC), 1-palmitoyl-2-oleoyl-*sn*-glycero-3-phosphoglycerol (POPG), 1,2-dipalmitoyl-*sn*-glycero-3- phosphocholine (DPPC), 1,2-dipalmitoyl-*sn*-glycero-3-phosphoglycerol (DPPG), 1,2-dipalmitoyl-*sn*-glycero-3-phosphoserine (DPPS), 1-palmitoyl-2-oleoyl-*sn*-glycero-3- phosphoethanolamine (POPE), 1,2-dioleoyl-*sn*-glycero-3-phosphocholine (DOPC), 1,2-dioleoyl-*sn*-glycero-3- phosphoglycerol (DOPG), palmitoyl sphingomyelin were purchased from Avanti Polar Lipids (Alabaster, AL). Cholesterol was purchased from Sigma Aldrich.

Liposome Preparation: Physical properties of (membrane fluidity & charge) of phago-endosomal membrane profile were mimicked based on the acyl chain composition and head group of the phospholipids [38–49] (Table 1). We mimicked the inner leaflet lipid raft after adding sphingomyelin and cholesterol to the raft composition (Table 1). Large unilamellar vesicles (LUVs) were prepared as described previously [32,33,50–52]. Briefly, individual phospholipids were dissolved in chloroform individually or were mixed as mentioned in Table 1. The lipids were first dried under a steady stream of nitrogen gas and left in vacuum overnight. The lipids were resuspended in 20 mM TrisHCl and 100 mM NaCl (pH 7.3) buffer through 6 freeze-thaw cycles in dry ice-ethanol mixture, followed by 15x extrusions in a mini-extruder (Avanti Polar Lipids) using 200 nm pore-size polycarbonate membranes. The final lipid concentration was 0.8 mM.

Protein Purification: The plasmid pMyNT-(EsxB:EsxA) was a generous gift from Dr. Matthias Wilmanns, which contains the native operon of *Mtb* EsxB:EsxA with a His_6-tag at the N-terminus of EsxB [53]. Using pMyNT-(EsxB:EsxA) as the template, the mutations of S35C and Q5K were introduced into EsxA gene by site-directed mutagenesis. The constructs pMyNT-(EsxB:EsxA(S35C)) and pMyNT-(EsxB:EsxA(Q5K/S35C) were transformed into *M. smegmatis* by electroporation at 2.5 kV. The bacterial colonies were grown in 7H9 plates supplemented with 10% OADC, 0.5% glycerol and 100 μg/ml of hygromycin. A single colony was picked and pre-cultured in 50 ml of 7H9 medium supplemented with 10% OADC, 0.5% glycerol, 0.05% Tween 80 and 100 μg/ml of hygromycin with shaking at 37 °C. The pre-culture was transferred to 1 l of 7H9 medium supplemented with 0.2% glycerol, 0.05% Tween 80, 0.2% glucose and 100 μg/ml of hygromycin to a final OD_{600} = 0.05 with shaking at 37 °C. Protein expression was induced at OD_{600} = 1.5 by adding acetamide (33 mM final concentration) for 48 h, and the cells were harvested by centrifugation. The pellet was lysed by sonication in the solubilization buffer (20 mM TrisHCl, 150 mM NaCl 10 mM imidazole, pH7.4), and the supernatant was collected by centrifugation at 15,200 × *g* for 1 h at 4 °C. The supernatant was loaded onto a Ni^{2+}-charged Sepharose column pre-equilibrated with the solubilization buffer. The bound proteins were eluted from the column by a linear gradient (10–100%) of the elution buffer (20 mM TrisHCl, 150 mM NaCl, 500 mM imidazole, pH7.4). The eluted heterodimer was further clarified through a gel filtration chromatography using a Sephadex 75 column in the gel filtration buffer (20 mM TrisHCl, 100 mM NaCl, pH 7.3).

Heterodimer Separation and NBD Labeling: The EsxB:EsxA(S35C) or EsxB:EsxA(Q5K/S35C) heterodimers were separated by 6 M guanidine. The solution was then concentrated to 1 ml and injected into a 5 ml Histrap column, which was pre-equilibrated with 25 mM NaH_2PO_4, 150 mM NaCl, 10 mM imidazole, 6 M guanidine. The His-tagged EsxB protein was bound to the column, while EsxA(S35C) and EsxA(Q5K/S35C) flew through the column. The EsxA proteins were collected and extensively dialyzed in 25 mM NaH_2PO_4, 100 mM NaCl, 1 mM EDTA. The dialyzed EsxA proteins were labeled with IANBD amide (*N*,*N*′-Dimethyl-*N*-(Iodoacetyl)-*N*′-(7-Nitrobenz-2-Oxa-1,3-Diazol-4-yl) Ethylenediamine) (Invitrogen) at the position S35C as previously described [33,36,50,51]. The labeling efficiency for both WT and Q5K was ~75%.

Intrinsic Tryptophan Fluorescence: The experiment was performed as previously described [32–34]. Briefly, 10 μM of the purified proteins were incubated either in a neutral pH buffer (20 mM TrisHCl, 100 mM NaCl, pH 7.0) or an acidic buffer (20 mM NaAc, 100 mM NaCl, pH 5.0) for 30 min. The intrinsic tryptophan fluorescence was measured in an ISS-K2 fluorometer with excitation at 295 nm and emission at 310–450 nm. A 305 nm long-pass filter was applied in the emission channel to reduce the background. The emission spectra of the proteins were corrected by subtracting the emission spectra of the buffers without proteins.

Circular Dichroism: A Jasco-1500 spectrofluoropolarimeter was used to conduct CD experiments with the samples placed in a 0.1-mm path

Table 1
The lipid compositions of the liposomes used in the study. The liposomes containing phagosome mimic lipids and lipid rafts were prepared with the indicated components. The unsaturation (%) and charge (%) of the lipids were indicated. The final unsaturation (%) and charge (%) of the liposomes were calculated.

				Composition (%) in liposomes		
Lipid name	# of carbon and double bond in fatty acid tails	% unsaturation	Net Charge	DOPC	Phagosome mimic	Lipid Raft
DOPC	2x (18:1)	100	0	100	0	0
POPC	16:0–18:1	50	0	0	65	35
DPPS	2x (16:0)	0	−1	0	20	15
POPE	16:0–18:1	50	0	0	15	20
Cholesterol	NA	NA	NA	0	0	15
Sphingomyelin	2x (16:0)	0	0	0	0	15
		Final Unsaturation (%)		100	40	27.5
		Net Charge (%)		0	−20	−15

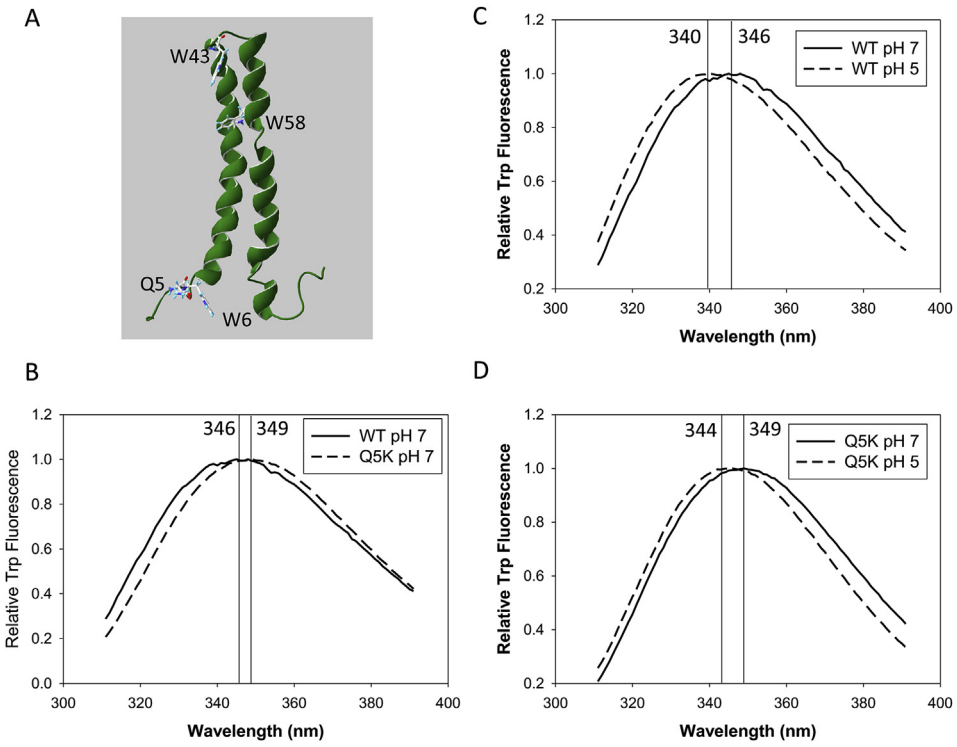

Fig. 1. Intrinsic Trp fluorescence of EsxA WT and Q5K in solution. A. The structure of EsxA is extracted from 1WA8 (PDB) and displayed in Swiss-PDB Viewer. The residues Q5, W6, W43 and W58 are shown. (**B-D**). 10 μM of EsxA WT and Q5K were incubated either at pH 7 or at pH 5 for 30 min. The samples were excited at 295 nm and the emission spectra of Trp fluorescence of the samples were recorded at 310–450 nm. The emission spectra of the proteins were corrected by subtracting the emission spectra of the buffers without proteins. The representative data from at least three independent experiments are shown in the figure. The wavelength at the peak of each spectrum is determined by fitting and smoothing the plots.

length quartz cuvette (Jasco). All the experiments were conducted in a final sample volume of 40 μl containing 100 μM of EsxA proteins in the absence or presence of 0.8 mM liposomes with the temperature ranging from 4 °C to 60 °C. At each temperature, the sample was pre-equilibrated for 5 min before measurements. The experimentally measured ellipticities (θ_{obs}) were converted to [θ], using the formula: $[\theta] = \theta_{obs}/cnl$. Here, c is the molar concentration of the protein, n is the number of amino acid residues in the protein and l is the path length of the cuvette in millimeters. The characteristic α-helical minimum at 208 nm was used to determine T_m values. Thermal unfolding profile was determined using a similar method as previously described [54–56]. EsxA's thermal unfolding profile were analyzed using the following equation:

$$X = f_L X_L + (1 - f_L) X_H \quad (1)$$

where X is the measured temperature-dependent change in ellipticity and f_L is the fraction of amino acids that are in native conformation at low temperature. X_L and X_H are the values at the lowest and highest temperatures respectively. f_L is further defined by:

$$f_L = \exp \frac{-\frac{\Delta G}{RT}}{\left[1 + \exp\left(-\frac{\Delta G}{RT}\right)\right]} \quad (2)$$

where the free energy of unfolding (ΔG) is defined by:

$$\Delta G = \Delta H\left(1 - \frac{T}{T_m}\right) + \Delta C\left[T - T_m - T\ln\left(\frac{T}{T_m}\right)\right] \quad (3)$$

here, T_m stands for protein melting temperature, ΔH is the apparent enthalpy for unfolding and ΔC is the heat capacity of unfolding. The value of ΔC = 0.39 kcal mol^{-1} K^{-1} and ΔH ranged between 34 and 40 kcal mol^{-1} were used to derive the best fit between experimental and simulated far UV curves. The temperature values in the table represents the average temperature calculated from three independent experiments with standard deviations. Our studies show that EsxA and its mutant become unstable at temperatures above 30 °C. To negate the time dependent effects of temperature, we minimized the number of steps for temperature change.

Time-lapse Intensity Measurement of NBD Emission: The NBD-labeled proteins (3 μM), either WT or Q5K, were incubated with 800 μM of the liposomes containing the indicated lipid compositions at 4 °C for 30 min in 20 mM TrisHCl and 100 mM NaCl pH 7.4 buffer. During incubation, we predict EsxA adsorbs over the surface of liposomes. By giving enough time for the proteins to interact and orient themselves over the lipid vesicles, we exclude the possibility that insertion of EsxA at pH 7.0 could be a time dependent process. Then the protein/liposome mixtures were transferred to a cuvette with a stirring bar in an ISS K2 fluorometer at RT. 0.1 volume of 1 M sodium acetate (pH 4) was added to drop the pH. The solution was continuously stirred while recording the data at RT. The emission spectra were recorded at 544 nm with excitation at 488 nm. Crossed polarizers on the excitation and emission beams and a 520 nm long-pass filter were used to reduce the background scatter. After the addition of 0.1 volume of 1 M sodium acetate (pH 4) to the cuvette, the NBD emission from a polar (solution) to a nonpolar (liposomal membrane) environment was monitored. All studies were conducted at RT. The fold change of NBD fluorescence intensity is calculated as $\Delta F/F_0 = (F_{final} - F_{initial})/F_{initial}$. $F_{initial}$ is the initial intensity prior to dropping pH, which stands for the background fluorescence signal. F_{final} is the highest intensity after dropping pH. To compare EsxA-NBD fluorescence among different lipids. We set EsxA-NBD in DOPC as 1.0 and compared it with all other intensities.

3. Results

Intrinsic Trp fluorescence of EsxA WT and Q5K mutant. Our previous study has found that Q5K mutation decreases the membrane-permeabilizing activity of EsxA and hence attenuates mycobacterial cytosolic translocation and virulence [36], but the mechanism is not clear. In order to test if the mutation affects the structure of EsxA, we first measured the intrinsic Trp fluorescence of WT and Q5K proteins at both pH 7 and pH 5. Tryptophan fluorescence studies are conducted as they are sensitive to the surrounding environment around the amino acid residue. If the tryptophan gets exposed to the solvent (water) we see a red shift and if it's in environment devoid of water, it is blue shifted. There are total three Trp residues in EsxA (Fig. 1A), and in our previous study, the measurement of intrinsic Trp fluorescence has

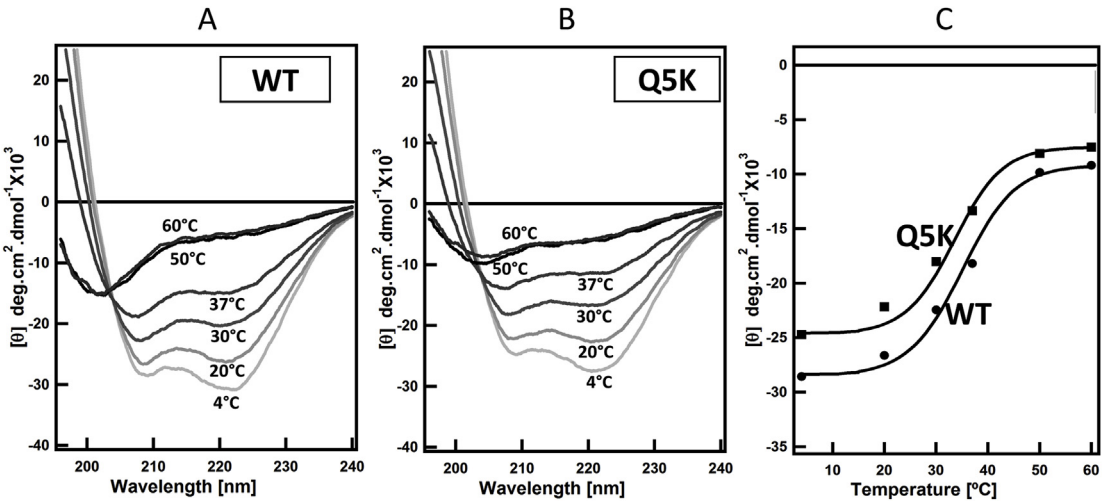

Fig. 2. Thermal unfolding profiles of WT and Q5K in solution. Far-UV CD measurements of the secondary structures of WT and Q5K (100 μM) were recorded in 20 mM Tris and 100 mM NaCl pH 7.4 buffer at the indicated temperatures. The spectra were shown in (**A** and **B**). The mean residue ellipticity at 208 nm (θ_{208}) was plotted as a function of temperature and shown in (**C**).

accurately reflected the pH-dependent conformational changes of EsxA [32–34]. At pH 7, the Trp spectrum of Q5K shows a similar shape with the spectrum of WT, but the spectral peak of Q5K is shifted ~3 nm to the right (Fig. 1B). Since the Q5K mutation is adjacent to the W6 residue, the observed shift could be due to the mutation that change the microenvironment of W6. Consistent with the previous result [32–34], upon acidification the Trp spectrum of WT exhibited a ~6 nm blue shift (Fig. 1C). Interestingly, however, the Q5K exhibits a ~5 nm blue shift, which is similar to WT, indicating that the Q5K mutation does not affect the pH-dependent conformational change (Fig. 1D).

Thermostability of WT and Q5K. To further explore the effects of the mutation on the overall structure of EsxA, we performed CD analysis to determine the thermostability of EsxA WT and the mutant. Using a Peltier temperature-controlled CD, we characterized the effect of temperature on the structural stability of EsxA WT and Q5K by itself. Far-UV CD analysis of the purified proteins was performed at various temperatures (4, 20, 30, 37, 50 and 60 °C, respectively). EsxA WT became unstable at the physiological temperature 37 °C, and the T_m of EsxA was calculated to be ~35 °C (Fig 2A, C and Table 2), which is similar to the early reported 33 °C and is consistent with the observation that EsxA is susceptible to degradation at physiological temperatures [57]. The T_m of Q5K is calculated as ~33.5 °C (Fig. 2B and C and Table 2). The Q5K mutation may slightly affect the thermal stability of EsxA protein in solution, but not in a significant way.

Next, we tested if the lipid membrane has any differential effect on the structures of WT and Q5K. As one of the common lipids for making liposomes, DOPC is regularly used to make liposomes in our previous studies of EsxA membrane interaction [32–34,36]. In the presence of DOPC liposomes, the average Tm values of WT and Q5K are 36.5 ± 0.6 °C and 35.5 ± 0.7 °C, respectively, which are slightly higher than their Tm values in solution (Fig. 3 (A-C) and Table 2), suggesting that DOPC may have a minor effect on stabilizing the structures of WT and Q5K. To simulate a more physiologically relevant membrane, we prepared the phagosome-mimic liposome (PM) and tested its effect on thermostability of WT and Q5K. The results show that the Tm values of WT and Q5K remain the same as in DOPC liposomes (Fig. 3 (D-F) and Table 2).

Lipid raft has been implicated in the pathogenesis of numerous bacterial pathogens by serving as the sites of cellular binding and entry for bacterial pathogens and pore-forming toxins [58–60]. Lipid raft has also been shown to be involved in Mtb infection [37,61]. Previous studies have shown perfringolysin, a pore forming toxin from *Clostridium perfringens*, has a high affinity towards raft-like membrane domains. Streptolysin O, which is another bacterial cytolysin, also has a high affinity towards raft-like membrane domains. Pore formation by both the toxins become less efficient when the rafts were disrupted [62,63]. There is a high propensity to find raft-like domains on phagosomal membrane. Is EsxA stabilized by raft-like domains on the membrane? Therefore, we tested the thermostability of WT and Q5K in the lipid raft-containing liposomes (Fig. 4 and Tables 1 and 2) and compared it to the phagosome-mimic liposomes, which does not have raft-like microdomains. In the presence of rafts, the T_m values of both WT and Q5K were 36.5 °C. (Fig. 4 and Table 2).

In summary, the lipid compositions tested in the study, including raft-like microdomain, have minimal effects on the structural stability of EsxA. The T_m values ranging between 33 and 36 °C in all experiments signify that EsxA remains essentially destabilized at physiological temperature even in the presence of various lipid compositions. The results also show that the Q5K mutation doesn't affect the pH-dependent conformational change and various lipid compositions don't discriminate between WT and Q5K in thermostability. Therefore, the defective membrane-permeabilizing activity of Q5K is not due to defects in structural stability.

Effects of lipid composition on EsxA membrane insertion. Since lipid composition has little effect on the thermostability of EsxA, it would be interesting to see if it affects EsxA membrane insertion. NBD, an environment-sensitive dye, emits fluorescence when it is shifted from an aqueous solution to a hydrophobic environment (e.g. lipid membranes). In our previous studies, NBD has been successfully used to measure membrane insertion of anthrax toxin [33,36,50,51,64]. Recently, using NBD-labeled EsxA proteins, we have confirmed that the

Table 2
Thermal unfolding profile of EsxA at $[\theta]_{208}$. Far-UV CD was used to determine structural stability of EsxA. The melting temperature for each sample is shown. The *Tm* values were calculated from at least three independent experiments.

Samples	T_m (°C)
EsxA (WT)	35 ± 0.4
EsxA (Q5K)	33.5 ± 0.3
EsxA (WT) + DOPC	36.5 ± 0.6
EsxA (Q5K) + DOPC	35.5 ± 0.7
EsxA (WT) + Phagosome mimic	36.5 ± 0.5
EsxA (Q5K) + Phagosome mimic	35.5 ± 0.5
EsxA (WT) + Lipid Raft	36.5 ± 0.4
EsxA (Q5K) + Lipid Raft	36.5 ± 0.6

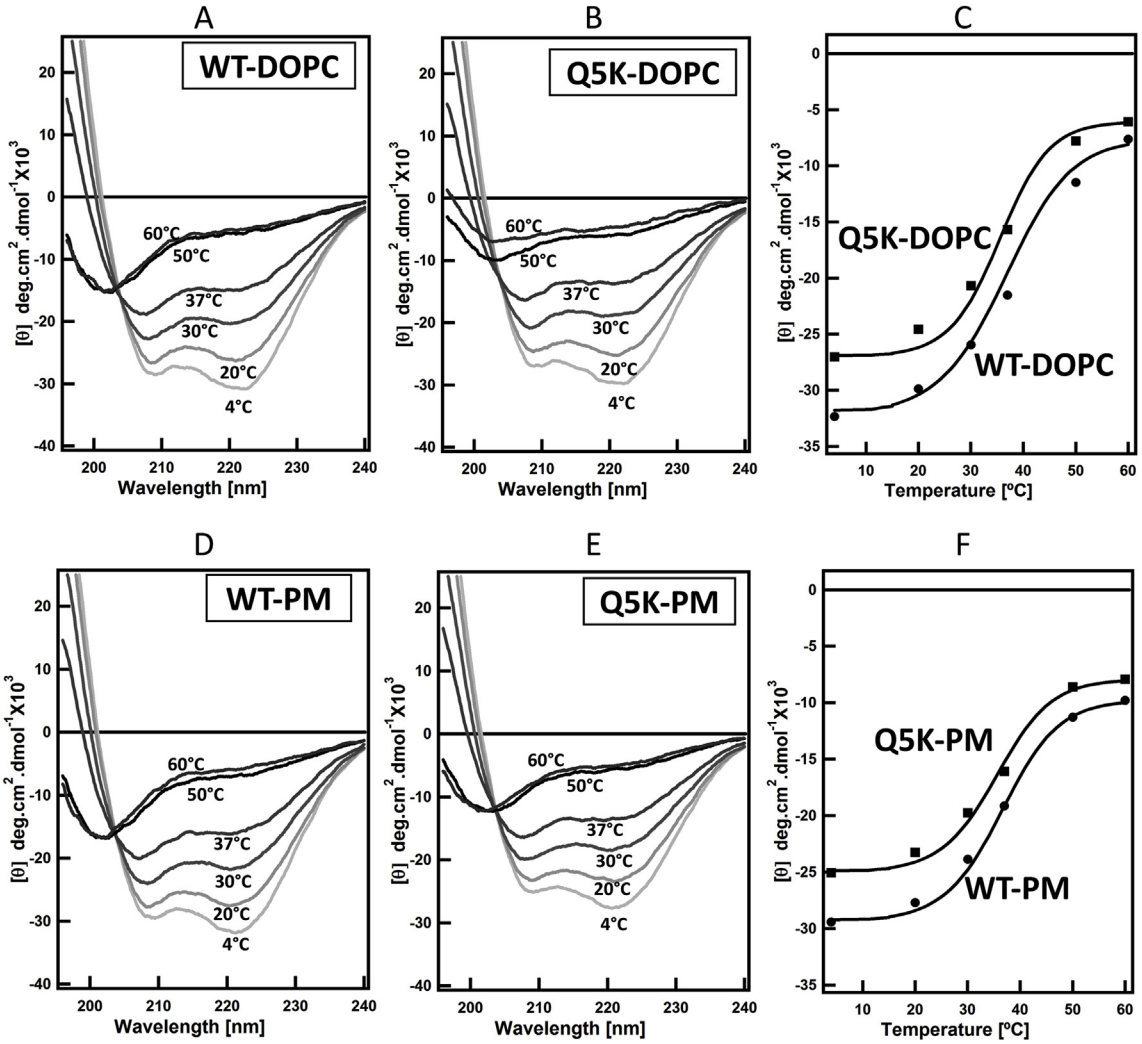

Fig. 3. Thermal unfolding profiles of WT and Q5K in liposomes made of DOPC and phagosome-mimic (PM) lipids. Far-UV CD measurements of the secondary structure of WT and Q5K proteins (100 μM) were recorded in 20 mM Tris and 100 mM NaCl pH 7.4 buffer at the indicated temperatures in the presence of 800 μM of the liposomes. The spectra are shown in (**A, B, D, E**). The mean residue ellipticity at 208 nm (θ_{208}) for both WT and Q5K were plotted as a function of temperature and shown in (**C** and **F**).

two α-helixes of EsxA insert into the DOPC membrane, while the N- and C-terminal loops stay outside the membrane [33]. Here, the NBD-labeled EsxA protein (NBD is labeled at S35C) was used to test EsxA insertion in the liposomal membranes containing various lipid compositions. Under the condition that the fluorescence of NBD does not depend significantly on the composition of the membrane, the intensity of the NBD fluorescence may be used to quantitatively compare the degree of insertion of EsxA in membranes of different lipid compositions. We found that the membrane insertion of EsxA was dramatically affected by different lipid compositions (Fig. 5). In the presence of the

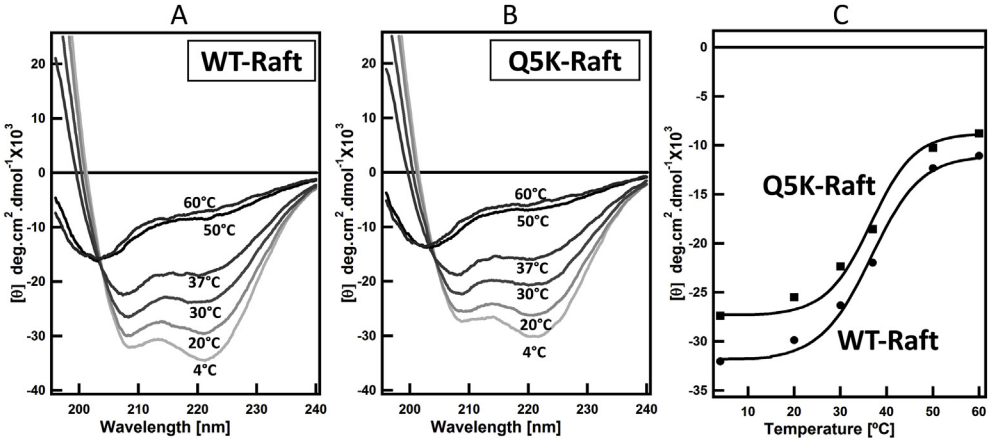

Fig. 4. Thermal unfolding profiles of WT and Q5K in the liposomes containing lipid raft. Far-UV CD measurements of the secondary structures of WT and Q5K (100 μM) were recorded in 20 mM Tris and 100 mM NaCl pH 7.4 buffer in the presence of 800 μM of the liposomes containing lipid raft. The spectra were shown in (**A, B**). The mean residue ellipticity at 208 nm (θ_{208}) for WT and Q5K was plotted as a function of temperature and shown in (**C**).

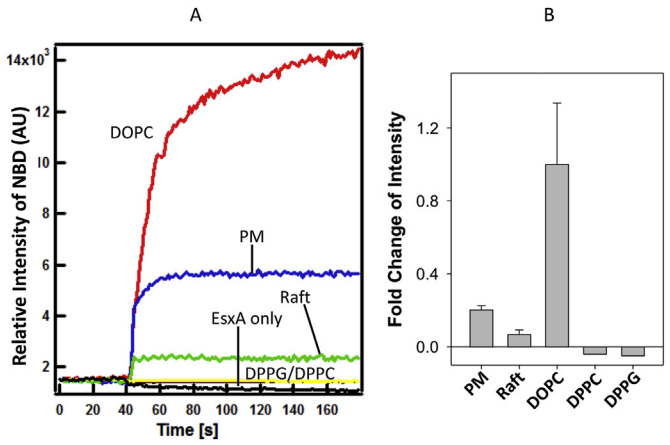

Fig. 5. Membrane insertion of EsxA was significantly affected by membrane unsaturation. The NBD-labeled EsxA WT (3 μM) was incubated with 800 μM of the liposomes containing the indicated lipid compositions (DOPC, DPPG, DPPC, lipid raft, phagosome mimic) at 4 °C for 30 min in 20 mM TrisHCl and 100 mM NaCl pH 7.4 buffer. Then the protein-liposome mixture was transferred at a cuvette at RT. 0.1 volume of 1 M sodium acetate (pH 4) was added to drop the pH. The solution was continuously stirred while recording the data at RT. The emission spectra were recorded at 544 nm with excitation at 488 nm and shown in (**A**). The fold change of fluorescence intensity relative to DOPC was shown in (**B**). EsxA without any liposome was used as a negative control. The representative data from 3 experiments are shown.

biologically relevant lipids, phagosome-mimic lipids or lipid rafts, EsxA membrane insertion activity was much lower than that in the model lipid DOPC. Since each of the DOPC fatty acid tails has one double bond, thus DOPC is highly unsaturated (here, defined as 100% unsaturation) (Table 3), while the biologically relevant liposomes have only 35–40% unsaturation (Table 1). The unsaturation level of fatty acids is a major factor affecting membrane fluidity. We hypothesize that membrane fluidity plays a role in EsxA membrane insertion. Moreover, DOPC liposomes have no net charge (100% neutral), while by calculation the liposomes made of phagosome-mimic lipids and lipid rafts have ~ 15–20% negative charge. Therefore, membrane charge may also play a role in EsxA insertion. To show that membrane fluidity is essential for EsxA insertion, we examined liposomes made of the saturated lipids DPPC and DPPG, which have a melting temperature of 41 °C and hence are in the solid phase at the experimental temperature. As expected, we observed no insertion of ExsA under these conditions. This also shows that the charge of the lipids is irrelevant to EsxA insertion when the membrane is not in a fluid phase (Fig. 5 and Table 3).

We also notice that the EsxA has a stronger insertion signal with the phagosome-mimic liposomes than the lipid raft liposomes (Fig. 5 and Table 3). It could be due to sphingomyelin that is highly saturated and can form ordered lipid microdomain (L_o) with cholesterol. Thus, lipid raft liposome is more ordered and rigid than the phagosome-mimic liposome.

To further dissect the relative roles of membrane fluidity and charge in EsxA membrane insertion, we compared DOPC (100% unsaturation, neutral), POPC (50% unsaturation, neutral), DOPG (100% unsaturation, 100% negative charge), and POPG (50% unsaturation, 100% negative charge). Compared to DOPC (set as 1.0), EsxA membrane insertion in DOPG, POPC, and POPG was 1.08, 0.45, and 1.9, respectively (Fig 6A, C and Table 3). At 100% membrane unsaturation, membrane charge (either neutral or 100% negative charge) does not affect membrane insertion (DOPC vs. DOPG). At 50% membrane unsaturation and neutral charge, membrane insertion is significantly reduced (DOPC vs. POPC), suggesting that the level of membrane unsaturation is an essential factor for membrane insertion. However, at 50% unsaturation and 100% negative charge, membrane insertion was remarkably increased (POPG), suggesting that at relatively reduced membrane unsaturation, membrane charge plays an important role in membrane insertion. Moreover, EsxA in the mixture of POPC:POPG (4:1) with 50% unsaturation and 20% negative charge showed a membrane insertion that was higher than that in DOPC, DOPG, POPC, but lower than that in POPG (Fig. 6A, C and Table 3). The physical properties (fluidity and charge) of the POPC:POPG (4:1) lipid mixture is closer to the physiological membranes. All the data suggest that EsxA membrane insertion is regulated by a complex dual play of membrane fluidity and charge.

There is a concern that fluorescence intensity of NBD is affected by both its location in the membrane (the depth) and the lipid compositions. To address the concern, we used the ANTS/DPX leakage assay to test the membrane-permeabilizing activity of EsxA WT in the liposomes made of DOPC, POPC or POPG, respectively (Fig. S1). The result shows that POPG has the highest leakage, which is followed by DOPC, and POPC has no leakage. While the overall intensity of ANTS/DPX fluorescence is lower than NBD, the relative intensity of ANTS/DPX in DOPC, POPC and POPG is consistent with the NBD result (Fig. 6A). It is worthy of mentioning that in our previous work (Fig. 1 in Ref. [36]), we tested both ANTS/DPX assay and NBD assay to compare WT and Q5K in DOPC membranes and obtained consistent results in the two assays. Therefore, the NBD assay and ANTSANTS/DPX assay are equivalent and reciprocally support each other in testing of EsxA membrane interactions.

To determine if Q5K is affected differentially than WT by membrane fluidity and charge, we used the same lipids above to test membrane insertion of Q5K. Overall, Q5K showed lower membrane insertion than WT in all the tested lipids (Fig. 6B and C and Table 3), which is consistent with the previous results [36].

We also measured the kinetics of NBD fluorescence (Table S1). We observed that upon dropping pH, the NBD fluorescence instantaneously increased and reached the maximum quickly. Consistent with the data in Fig. 6, the Vmax values of WT in different lipids are generally larger than Q5K, except for POPC, in which WT and Q5K are similar. While the h values (coefficient of protein-lipid interaction) show an opposite pattern compared to Vmax. That is, the h values of Q5K are larger than WT in the corresponding lipids, except for POPC that Q5K has a smaller h value than WT. This suggests that while Q5K has a more stable

Table 3
Effects of membrane unsaturation and charge on membrane insertion of WT and Q5K. The data of membrane insertion of WT and Q5K in the presence of various lipids were collected from Figs. 6 and 5. Membrane insertion of WT in DOPC was set as 1.0, and all other data were compared to WT in DOPC.

Lipids	# of carbon and double bond in fatty acid tails	Unsaturation (%)	Phase Transition Temperature (°C)	Net-Charge/lipid molecule	Membrane insertion of WT	Membrane insertion of Q5K
DOPC	2x (18:1)	100	−17	0	1	0.63
DOPG	2x (18:1)	100	−18	−1	1.08	0.52
POPC	16:0–18:1	50	−2	0	0.45	0.30
POPG	16:0–18:1	50	−2	−1	1.90	0.90
POPC(4):POPG(1)	16:0–18:1	50	−2	80% neutral:20% negative	1.4	0.90
DPPC	2x (16:0)	0	41	0	ND	ND
DPPG	2x (16:0)	0	41	−1	ND	ND

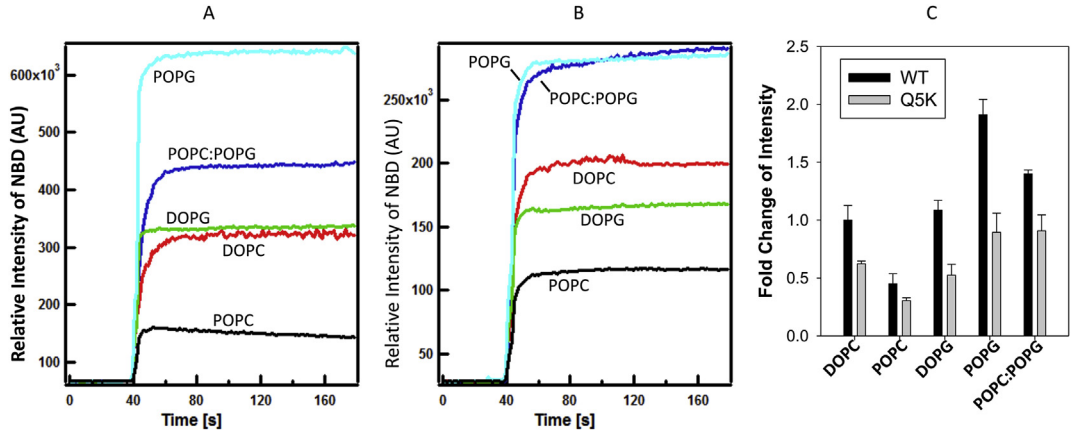

Fig. 6. Membrane insertion of EsxA is affected by both membrane unsaturation and charge. The NBD-labeled WT and Q5K were incubated with 800 μM of the indicated liposomes at 4 °C for 30 min in 20 mM TrisHCl and 100 mM NaCl pH 7.4 buffer. The protein-liposome mixture was transferred into a cuvette at RT. 0.1 volume of 1 M sodium acetate (pH 4) was added to drop the pH. The solution was continuously stirred while recording the data at RT. The emission spectra were recorded at 544 nm with excitation at 488 nm, and the representative spectra are shown in (**A**) for WT and (**B**) for Q5K. The fold changes relative to DOPC were shown in (**C**).

interaction with the lipids, but it has a lower efficiency to insert into the membrane. The $K_{0.5}$ values (the half time to reach 50% Vmax) are similar between WT and Q5k in all of the tested lipids, except for DOPG, suggesting that the rate of membrane insertion is similar between WT and Q5K, and the major difference between WT and Q5K is the amounts of proteins inserting into the membrane upon acidification. The $K_{0.5}$ value of Q5K is 10s longer than that of WT, which is presumably due to the interaction between the negative charge of DOPG and the positive charge of Q5K that delays the rate of membrane insertion.

4. Discussion

In the present study, the intrinsic Trp fluorescence measurements suggest that the Q5K mutation doesn't appear to affect the pH-dependent conformational changes (Fig. 1). This data is supported by the CD analysis of thermostability, in which Q5K has a slightly lower Tm than WT in solution (Fig. 2 and Table 2). In comparison of the thermostability of WT and Q5K in different lipid compositions, we did not observe any significant difference in their Tm values (Figs. 3 and 4 and Table 2), indicating that the defect of Q5K in membrane insertion is not caused by structural defects in different contexts of lipids. Moreover, various lipid compositions didn't have apparent differential effects on the membrane insertion between WT and Q5K, evidenced by the results that despite of various lipid compositions, Q5K consistently exhibited lower membrane insertion than WT (Fig. 6 and Table 3). Thus, the defect of Q5K in membrane insertion is independent of lipid compositions. This observation is consistent with the finding in our early study using the NBD-labeled EsxA proteins, in which we have found that both α-helices of EsxA insert into the membrane, but the N- and C-terminal arms don't insert into the membranes [33]. Therefore, all of the data suggest that the effects of Q5 mutations on EsxA membrane insertion are achieved neither through altering the structure of the membrane-inserting α-helices of EsxA, nor through directly interacting with the lipids. This study has inspired us to propose that Q5 plays a role in EsxA oligomerization during pore formation on the membrane, where the N- and C-terminal arms stabilize the oligomeric pore by binding each other in an intermolecular “head-to-tail” interaction.

The Tm of EsxA WT in aqueous solution is ~35 °C (Table 2), which is similar to the early reported 33 °C [57]. The Tm of the heterodimer was reported to be 53 °C [57]. The data suggest that at the physiological temperature 37 °C, EsxA is partly unfolded unless it is bound by EsxB. We have also found that EsxA is more active in membrane disruption at 37 °C than at RT, indicating that a partly unfolded EsxA is preferred for membrane insertion. Together, the data support the model that EsxA is stabilized by EsxB within the heterodimer until it is released from EsxB and then becomes partly unfolded for membrane insertion.

Using the NBD-labeled EsxA proteins, we can directly monitor the physical insertion of EsxA into lipid membranes. To our surprise, EsxA membrane insertion in DOPC liposome is significantly higher than that in phagosome mimic lipids or lipid raft (Fig. 5). This observation has inspired us to investigate the potential effects of membrane fluidity and charge on EsxA membrane insertion (Fig. 6). As we have expected, the data clearly show that the membrane fluidity due to lipid unsaturation is required for EsxA membrane insertion, which is similar to the recent finding that the membrane-lytic efficiency of EsxA is decreased in more rigid membranes [65]. Moreover, numerous earlier studies of bacterial pore-forming toxins have shown that fluid lipid membranes are permeabilized more readily than less fluid, ordered membranes [59,66,67]. Together, these findings continuously support the notion that EsxA functions as a pore-forming protein that requires membrane fluidity for membrane insertion. Interestingly, the membrane charge also plays an important role in modulating EsxA membrane insertion (Fig. 6 and Table 3). At 50% unsaturation, the charge is positively correlated to membrane insertion (Refer to POPC:POPG (4:1) and POPG in Table 3). It could be because that upon acidification the protonated EsxA residues have a better interaction with the negatively charged lipids. However, DOPG (100% unsaturation and 100% negative charge) does not increase membrane insertion compared to DOPC (100% unsaturation, no charge). Moreover, membrane insertion in DOPG is nearly 50% lower than that in POPG (50% unsaturation and 100% negative charge), suggesting that high unsaturation level in the presence of charge may have negative effect on EsxA membrane insertion. The complex dual regulation of EsxA membrane insertion by membrane fluidity and charge warrants further investigation in future.

Recently, Conrad et al. have reported that the recombinant EsxA does not lyse cell membranes, and the lytic activity previously attributed to EsxA is due to residual detergent in the preparation [68]. In addition, the report also shows that the detergent-free EsxA does lyse the DOPC liposome at acidic pH, which has confirmed the results published by our group [32,33]. Moreover, in Conrad's report, the detergent-free EsxA is essentially inactive in hemolysis of sheep RBCs. It is known that sheep RBCs have 52% sphingomyelin, which is the one of the highest sphingomyelin content among the mammalian RBCs [69,70]. High content of sphingomyelin is associated with high membrane rigidity, especially upon interaction with cholesterol to form ordered raft microdomain. Thus, the results in sheep RBCs in Conrad's report are consistent with the results shown in Fig. 5. It is clear that EsxA membrane-lytic activity is dependent on lipid compositions (e.g.

fluidity and charge). Based on current data, however, the role of EsxA in phagosome rupture and cytosolic translocation is still not clear. Our previous studies have found that EsxA lyses DOPC liposomes at acidic pH [32–34], and the mutations at Q5 (e.g. Q5K, Q5V) down- or up-regulate the membrane-lytic activity of EsxA in DOPC liposomes, and these mutations down- or up-regulate mycobacterial cytosolic translocation and virulence accordingly [36], which strongly indicates a close link between EsxA membrane-lytic activity with mycobacterial cytosolic translocation and virulence. Correlated to this finding, the present study shows that the Q5K mutant consistently exhibits lower membrane-lytic activity than WT in various lipid compositions (Fig. 6). Interestingly, however, the Conrad's report has found that mycobacteria lyse cell membranes in a ESX-1-dependent and contact-dependent manner and can proceed at neutral pH [68]. It is possible that other factors from mycobacteria (e.g. PDIM [65]) or host are involved in ESX-1-mediated membrane lysis, which requires further investigation.

Author contribution

S Ray, XC and JS conceived and designed the study. S Ray and S Reyes performed the experiments. S Ray, S Reyes and JS wrote the manuscript. JS supervised the study.

Conflict of interest

The authors declare that they have no conflicts of interest with the contents of this article.

Acknowledgements

We thank Dr. Matthias Wilmanns for providing the pMyNT plasmid. The study is supported by the grants from National Institute of General Medical Sciences, United States (NIGMS grant SC1GM095475 to J. Sun), National Center for Research Resources, United States, (5G12RR008124) and National Institute on Minority Health and Health Disparities, United States (G12MD007592). Some of this work and S. Ray were supported by NIGMS grants (RL5GM118969, TL4GM118971, UL1GM118970). The content is solely the responsibility of the authors and does not necessarily represent the official views of the National Institutes of Health.

Appendix A. Supplementary data

Supplementary data to this article can be found online at https://doi.org/10.1016/j.tube.2019.07.005.

References

[1] WHO. Global tuberculosis report 2018. 2018.
[2] Zumla A, Raviglione M, Hafner R, Fordham von Reyn C. Tuberculosis. N. Engl. J. Med. 2013;368:745–55.
[3] Pethe K, Swenson DL, Alonso S, Anderson J, Wang C, Russell DG. Isolation of Mycobacterium tuberculosis mutants defective in the arrest of phagosome maturation. Proc Natl Acad Sci USA 2004;101:13642–7.
[4] Tan T, Lee WL, Alexander DC, Grinstein S, Liu J. The ESAT-6/CFP-10 secretion system of Mycobacterium marinum modulates phagosome maturation. Cell Microbiol 2006;8:1417–29.
[5] Orme I. Adaptive immunity to mycobacteria. Curr Opin Microbiol 2004;7:58–61.
[6] Kang PB, Azad AK, Torrelles JB, Kaufman TM, Beharka A, Tibesar E, DesJardin LE, Schlesinger LS. The human macrophage mannose receptor directs Mycobacterium tuberculosis lipoarabinomannan-mediated phagosome biogenesis. J Exp Med 2005;202:987–99.
[7] Pizarro-Cerdá J, Cossart P. Bacterial adhesion and entry into host cells. Cell 2006;124:715–27.
[8] van der Wel N, Hava D, Houben D, Fluitsma D, van Zon M, Pierson J, Brenner M, Peters PJ. M. tuberculosis and M. leprae translocate from the phagolysosome to the cytosol in myeloid cells. Cell 2007;129:1287–98.
[9] Houben D, Demangel C, van Ingen J, Perez J, Baldeón L, Abdallah AM, Caleechurn L, Bottai D, van Zon M, De Punder K, van der Laan T, Kant A, Bossers-de Vries R, Willemsen P, Bitter W, van Soolingen D, Brosch R, van der Wel N, Peters PJ. ESX-1 mediated translocation to the cytosol controls virulence of mycobacteria. Cell Microbiol 2012;14:1287–98.
[10] Simeone R, Sayes F, Song O, Gröschel MI, Brodin P, Brosch R, Majlessi L. Cytosolic access of Mycobacterium tuberculosis: critical impact of phagosomal acidification control and demonstration of occurrence in vivo. PLoS Pathog 2015;11:e1004650.
[11] Simeone R, Bottai D, Brosch R. ESX/type VII secretion systems and their role in host-pathogen interaction. Curr Opin Microbiol 2009;12:4–10.
[12] Simeone R, Bobard A, Lippmann J, Bitter W, Majlessi L, Brosch R, Enninga J. Phagosomal rupture by Mycobacterium tuberculosis results in toxicity and host cell death. PLoS Pathog 2012;8:e1002507.
[13] MacGurn JA, Cox JS. A genetic screen for Mycobacterium tuberculosis mutants defective for phagosome maturation arrest identifies components of the ESX-1 secretion system. Infect Immun 2007;75:2668–78.
[14] Stanley SA, Raghavan S, Hwang WW, Cox JS. Acute infection and macrophage subversion by Mycobacterium tuberculosis require a specialized secretion system. Proc Natl Acad Sci USA 2003;100:13001–6.
[15] Mahairas GG, Sabo PJ, Hickey MJ, Singh DC, Stover CK. Molecular analysis of genetic differences between Mycobacterium bovis BCG and virulent M. bovis. J Bacteriol 1996;178:1274–82.
[16] Behr MA, Wilson MA, Gill WP, Salamon H, Schoolnik GK, Rane S, Small PM. Comparative genomics of BCG vaccines by whole-genome DNA microarray. Science 1999;284:1520–3.
[17] Pym AS, Brodin P, Brosch R, Huerre M, Cole ST. Loss of RD1 contributed to the attenuation of the live tuberculosis vaccines Mycobacterium bovis BCG and Mycobacterium microti. Mol Microbiol 2002;46:709–17.
[18] Pym AS, Brodin P, Majlessi L, Brosch R, Demangel C, Williams A, Griffiths KE, Marchal G, Leclerc C, Cole ST. Recombinant BCG exporting ESAT-6 confers enhanced protection against tuberculosis. Nat Med 2003;9:533–9.
[19] Hsu T, Hingley-Wilson SM, Chen B, Chen M, Dai AZ, Morin PM, Marks CB, Padiyar J, Goulding C, Gingery M, Eisenberg D, Russell RG, Derrick SC, Collins FM, Morris SL, King CH, William R Jacobs J. The primary mechanism of attenuation of bacillus Calmette–Guérin is a loss of secreted lytic function required for invasion of lung interstitial tissue. Proc Natl Acad Sci USA 2003;100:12420–5.
[20] Lewis KN, Liao R, Guinn KM, Hickey MJ, Smith S, Behr MA, Sherman DR. Deletion of RD1 from Mycobacterium tuberculosis mimics bacille Calmette-Guérin attenuation. J Infect Dis 2003;187:117–23.
[21] Sassetti CM, Rubin EJ. Genetic requirements for mycobacterial survival during infection. Proc Natl Acad Sci USA 2003;100:12989–94.
[22] Guinn KM, Hickey MJ, Mathur SK, Zakel KL, Grotzke JE, Lewinsohn DM, Smith S, Sherman DR. Individual RD1-region genes are required for export of ESAT-6/CFP-10 and for virulence of Mycobacterium tuberculosis. Mol Microbiol 2004;51:359–70.
[23] Andersen P, Andersen AB, Sørensen AL, Nagai S. Recall of long-lived immunity to Mycobacterium tuberculosis infection in mice. J Immunol 1995;154:3359–72.
[24] Berthet FX, Rasmussen PB, Rosenkrands I, Andersen P, Gicquel B. A Mycobacterium tuberculosis operon encoding ESAT-6 and a novel low-molecular-mass culture filtrate protein (CFP-10). Microbiology 1998;144(Pt 11):3195–203.
[25] Harboe M, Oettinger T, Wiker HG, Rosenkrands I, Andersen P. Evidence for occurrence of the ESAT-6 protein in Mycobacterium tuberculosis and virulent Mycobacterium bovis and for its absence in Mycobacterium bovis BCG. Infect Immun 1996;64:16–22.
[26] Nagai S, Wiker HG, Harboe M, Kinomoto M. Isolation and partial characterization of major protein antigens in the culture fluid of Mycobacterium tuberculosis. Infect Immun 1991;59:372–82.
[27] Fortune SM, Jaeger A, Sarracino DA, Chase MR, Sassetti CM, Sherman DR, Bloom BR, Rubin EJ. Mutually dependent secretion of proteins required for mycobacterial virulence. Proc Natl Acad Sci USA 2005;102:10676–81.
[28] The Tuberculosis Vaccines Pipeline: A New Path to the Same Destination?. The tuberculosis vaccines pipeline: a new path to the same destination? 2017.
[29] Brennan MJ, Thole J. Tuberculosis vaccines: a strategic blueprint for the next decade. Tuberculosis 2012;92:S6–13.
[30] Hoang T, Aagaard C, Dietrich J, Cassidy JP, Dolganov G, Schoolnik GK, Lundberg CV, Agger EM, Andersen P. ESAT-6 (EsxA) and TB10.4 (EsxH) based vaccines for pre- and post-exposure tuberculosis vaccination. PLoS One 2013;8:e80579.
[31] de Jonge MI, Pehau-Arnaudet G, Fretz MM, Romain F, Bottai D, Brodin P, Honoré N, Marchal G, Jiskoot W, England P, Cole ST, Brosch R. ESAT-6 from mycobacterium tuberculosis dissociates from its putative chaperone CFP-10 under acidic conditions and exhibits membrane-lysing activity. J Bacteriol 2007;189:6028–34.
[32] De Leon J, Jiang G, Ma Y, Rubin E, Fortune S, Sun J. Mycobacterium tuberculosis ESAT-6 exhibits a unique membrane-interacting activity that is not found in its ortholog from non-pathogenic Mycobacterium smegmatis. J Biol Chem 2012;287:44184–91.
[33] Ma Y, Keil V, Sun J. Characterization of Mycobacterium tuberculosis EsxA membrane insertion: roles of N- and C-terminal flexible arms and central helix-turn-helix motif. J Biol Chem 2015;290:7314–22.
[34] Peng X, Jiang G, Liu W, Zhang Q, Qian W, Sun J. Characterization of differential pore-forming activities of ESAT-6 proteins from Mycobacterium tuberculosis and Mycobacterium smegmatis. FEBS Lett 2016;590:509–19.
[35] Peng X, Sun J. Mechanism of ESAT-6 membrane interaction and its roles in pathogenesis of Mycobacterium tuberculosis. Toxicon 2016;116:29–34.
[36] Zhang Q, Wang D, Jiang G, Liu W, Deng Q, Li X, Qian W, Ouellet H, Sun J. EsxA membrane-permeabilizing activity plays a key role in mycobacterial cytosolic translocation and virulence: effects of single-residue mutations at glutamine 5. Sci Rep 2016;6:32618.
[37] Fine-Coulson K, Reaves BJ, Karls RK, Quinn FD. The role of lipid raft aggregation in the infection of type II pneumocytes by Mycobacterium tuberculosis. PLoS One 2012;7:e45028.

[38] van der Goot FG, Gruenberg J. Intra-endosomal membrane traffic. Trends Cell Biol 2006;16:514–21.
[39] Bissig C, Gruenberg J. Lipid sorting and multivesicular endosome biogenesis. Cold Spring Harbor Perspect Biol 2013;5:a016816.
[40] Gruenberg J. Lipids in endocytic membrane transport and sorting. Curr Opin Cell Biol 2003;15:382–8.
[41] Kobayashi T, Beuchat M-H, Chevallier J, Makino A, Mayran N, Escola J-M, Lebrand C, Cosson P, Kobayashi T, Gruenberg J. Separation and characterization of late endosomal membrane domains. J Biol Chem 2002;277:32157–64.
[42] Bissig C, Johnson S, Gruenberg J. Studying lipids involved in the endosomal pathway. Methods Cell Biol 2012;108:19–46.
[43] Guha S, Rajani M, Padh H. Identification and characterization of lipids from endosomes purified by electromagnetic chromatography. Indian J Biochem Biophys 2007;44:443–9.
[44] Chroneos ZC, Midde K, Sever-Chroneos Z, Jagannath C. Pulmonary surfactant and tuberculosis. Tuberculosis 2009;89(Suppl 1). S10–4.
[45] Nüsse O. Biochemistry of the phagosome: the challenge to study a transient organelle. Sci World J 2011;11:2364–81.
[46] Schmitz G, Müller G. Structure and function of lamellar bodies, lipid-protein complexes involved in storage and secretion of cellular lipids. J Lipid Res 1991;32:1539–70.
[47] van Meer G, Voelker DR, Feigenson GW. Membrane lipids: where they are and how they behave. Nat Rev Mol Cell Biol 2008;9:112–24.
[48] Sprong H, van der Sluijs P, van Meer G. How proteins move lipids and lipids move proteins. Nat Rev Mol Cell Biol 2001;2:504–13.
[49] Vanni S, Hirose H, Barelli H, Antonny B, Gautier R. A sub-nanometre view of how membrane curvature and composition modulate lipid packing and protein recruitment. Nat Commun 2014;5:4916.
[50] Sun J, Vernier G, Wigelsworth DJ, Collier RJ. Insertion of anthrax protective antigen into liposomal membranes: effects of a receptor. J Biol Chem 2007;282:1059–65.
[51] Sun J, Lang AE, Aktories K, Collier RJ. Phenylalanine-427 of anthrax protective antigen functions in both pore formation and protein translocation. Proc Natl Acad Sci USA 2008;105:4346–51.
[52] Sun J, Collier RJ. Disulfide bonds in the ectodomain of anthrax toxin receptor 2 are required for the receptor-bound protective-antigen pore to function. PLoS One 2010;5:e10553.
[53] Poulsen C, Holton S, Geerlof A, Wilmanns M, Song Y-H. Stoichiometric protein complex formation and over-expression using the prokaryotic native operon structure. FEBS Lett 2010;584:669–74.
[54] Ray S, Taylor M, Banerjee T, Tatulian SA, Teter K. Lipid rafts alter the stability and activity of the cholera toxin A1 subunit. J Biol Chem 2012;287:30395–405.
[55] Ray S, Taylor M, Burlingame M, Tatulian SA, Teter K. Modulation of toxin stability by 4-phenylbutyric acid and negatively charged phospholipids. PLoS One 2011;6:e23692.
[56] Lavigne P, Crump MP, Gagné SM, Hodges RS, Kay CM, Sykes BD. Insights into the mechanism of heterodimerization from the 1H-NMR solution structure of the c-Myc-Max heterodimeric leucine zipper. J Mol Biol 1998;281:165–81.
[57] Meher AK, Bal NC, Chary KVR, Arora A. Mycobacterium tuberculosis H37Rv ESAT-6-CFP-10 complex formation confers thermodynamic and biochemical stability. FEBS J 2006;273:1445–62.
[58] Vieira FS, Corrêa G, Einicker-Lamas M, Coutinho-Silva R. Host-cell lipid rafts: a safe door for micro-organisms? Biol Cell 2010;102:391–407.
[59] Rojko N, Anderluh G. How lipid membranes affect pore forming toxin activity. Acc Chem Res 2015;48:3073–9.
[60] Morante K, Caaveiro JMM, Tanaka K, González-Mañas JM, Tsumoto K. A pore-forming toxin requires a specific residue for its activity in membranes with particular physicochemical properties. J Biol Chem 2015;290:10850–61.
[61] Shin D-M, Yang C-S, Lee J-Y, Lee SJ, Choi H-H, Lee H-M, Yuk J-M, Harding CV, Jo E-K. Mycobacterium tuberculosis lipoprotein-induced association of TLR2 with protein kinase C zeta in lipid rafts contributes to reactive oxygen species-dependent inflammatory signalling in macrophages. Cell Microbiol 2008;10:1893–905.
[62] Nelson LD, Johnson AE, London E. How interaction of perfringolysin O with membranes is controlled by sterol structure, lipid structure, and physiological low pH: insights into the origin of perfringolysin O-lipid raft interaction. J Biol Chem 2008;283:4632–42.
[63] Ogasawara F, Kano F, Murata M, Kimura Y, Kioka N, Ueda K. Changes in the asymmetric distribution of cholesterol in the plasma membrane influence streptolysin O pore formation. Sci Rep 2019. https://doi.org/10.1038/s41598-019-39973-x.
[64] Jacquez P, Avila G, Boone K, Altiyev A, Puschhof J, Sauter R, Arigi E, Ruiz B, Peng X, Almeida I, Sherman M, Xiao C, Sun J. The disulfide bond Cys255-Cys279 in the immunoglobulin-like domain of anthrax toxin receptor 2 is required for membrane insertion of anthrax protective antigen pore. PLoS One 2015;10:e0130832.
[65] Augenstreich J, Arbues A, Simeone R, Haanappel E, Wegener A, Sayes F, Chevalier FL, Chalut C, Malaga W, Guilhot C, Brosch R, Astarie-Dequeker C. ESX-1 and phthiocerol dimycocerosates of Mycobacterium tuberculosis act in concert to cause phagosomal rupture and host cell apoptosis. Cell Microbiol 2017;19:e12726.
[66] Tomita T, Watanabe M, Yasuda T. Effect of fatty acyl domain of phospholipids on the membrane-channel formation of Staphylococcus aureus alpha-toxin in liposome membrane. Biochim Biophys Acta 1992;1104:325–30.
[67] Tomita T, Watanabe M, Yasuda T. Influence of membrane fluidity on the assembly of Staphylococcus aureus alpha-toxin, a channel-forming protein, in liposome membrane. J Biol Chem 1992;267:13391–7.
[68] Conrad WH, Osman MM, Shanahan JK, Chu F, Takaki KK, Cameron J, Hopkinson-Woolley D, Brosch R, Ramakrishnan L. Mycobacterial ESX-1 secretion system mediates host cell lysis through bacterium contact-dependent gross membrane disruptions. Proc Natl Acad Sci USA 2017;114:1371–6.
[69] Milhas D, Clarke CJ, Hannun YA. Sphingomyelin metabolism at the plasma membrane: implications for bioactive sphingolipids. FEBS Lett 2010;584:1887–94.
[70] Virtanen JA, Cheng KH, Somerharju P. Phospholipid composition of the mammalian red cell membrane can be rationalized by a superlattice model. Proc Natl Acad Sci USA 1998;95:4964–9.